




Design and validation of a fission-product source for radioactive beams

J. Song ^{1,*}, G. Savard ^{1,2}, J. Greene ¹ and J. A. Nolen ^{1,†}

¹Physics Division, Argonne National Laboratory, Lemont, Illinois 60439, USA

²Department of Physics, University of Chicago, Chicago, Illinois 60637, USA

 (Received 18 March 2022; revised 22 March 2023; accepted 16 January 2024; published 12 February 2024)

A neutron-generator-based source of fission products (nuCARIBU) is being developed to replace the existing ^{252}Cf source at Argonne National Laboratory. Neutrons generated by ${}^7\text{Li}(p, n){}^7\text{Be}$ reaction are thermalized in a compact polyethylene $[(\text{C}_2\text{H}_4)_n]$ moderator and impinge on a thin ^{235}U foil to produce fission products. Experiments have been conducted to verify the nuCARIBU concept and simulation results using a 4 MeV, 0.16 μA proton beam from the ATLAS accelerator irradiating a LiF neutron production target and two different simplified versions of the nuCARIBU $(\text{C}_2\text{H}_4)_n$ moderator with thicknesses of 3.81 cm and 1.91 cm separating it from the enriched ^{235}U fission foil. The emitted γ -ray peaks of 1383.93 keV (^{92}Sr), 358.0 keV (^{104}Tc), 565.992 keV (^{134}Te), and 258.411 keV (^{138}Xe) obtained from fission products are used to determine the neutron-induced fission rates in the fission foil. The measured fission rates are in good agreement with those simulated using the PHITS Monte Carlo code with user-defined neutron production cross sections based on well-known cross section data. These experimental results, consistent with the simulations, show that the current ^{252}Cf source (CARIBU) can be replaced by the neutron induced fission source (nuCARIBU).

DOI: [10.1103/PhysRevC.109.024605](https://doi.org/10.1103/PhysRevC.109.024605)

I. INTRODUCTION

Our understanding of the structure and reactions of neutron-rich nuclei lying far from the valley of the β stability has improved in the last few decades, driven by various experimental results from radioactive ion beam facilities. These facilities have historically been categorized into two main types, the isotope separation on line (ISOL) and in-flight fragment separator types, based on the production and extraction mechanisms used. About a decade ago, a new type of facility emerged with the development at Argonne National Laboratory of the californium rare isotope breeder upgrade (CARIBU) [1–3]. CARIBU uses a novel gas catcher system to transform fission products from ^{252}Cf fission into a high-quality beam of radioactive ions that are purified by mass separation and further manipulated to produce neutron-rich low-energy and reaccelerated beams. Furthermore, it provides short-lived rare isotope beams not typically delivered by ISOL-type facilities. CARIBU successfully provides beams of ^{252}Cf fission products to a large community of users for mass measurement and decay studies related to nuclear structure and astrophysics, in addition to world-unique programs in Coulomb excitation of refractory or otherwise difficult neutron-rich rare isotope beams in particular in the $A \approx 100$ and $N \approx 100$ regions [4–11].

The use of a strong ^{252}Cf spontaneous fission source to generate the initial fission products allowed these physics programs to be initiated without the need for an additional

accelerator to produce the fission products. However ^{252}Cf has a half-life of 2.6 y which means the source has to be replaced every three years or so and procuring replacement thin 1 Ci sources has proven to be difficult and unreliable. A new approach is required to improve these issues. It is now proposed to increase the radioactive beam capabilities of the ATLAS/CARIBU accelerator facility by the installation of a new source of fission products in CARIBU (called nuCARIBU) to provide a more reliable and intense source of short-lived neutron-rich isotopes [12] (see Appendix). With nuCARIBU, the neutron-generator-based source will resolve the issues caused by using the ^{252}Cf foil while making the system easier to maintain and operate since the main source of radioactivity will now be able to be turned off.

Simplified layouts of beam production at CARIBU and nuCARIBU are presented in Fig. 1. At CARIBU (Fig. 1(a)), the fission products are obtained from the spontaneous fission of a thin ^{252}Cf source whose fission products are stopped in a large gas catcher and extracted as a cooled low-energy beam. The nuCARIBU will use a similar extraction method but will use fission products generated by neutron induced fission on a thin ^{235}U foil, with the neutrons produced by a thermal neutron generator adjoined to the gas catcher (Fig. 1(b)). The proposed ${}^7\text{Li}(p, n)$ based neutron generator will produce an intense thermal neutron flux at the actinide foil, resulting in a fission rate exceeding that available at CARIBU by roughly an order of magnitude. The neutron-induced fission product mass distribution of ^{235}U is considerably shifted from that from spontaneous fission of ^{252}Cf (see Fig. 1(c)), with large gains in the mass regions $A < 100$ and $120 < A < 150$, and some losses for the heaviest part of both fission peaks. This will yield significant advantages for programs such as

*songj@anl.gov

†nolen@anl.gov

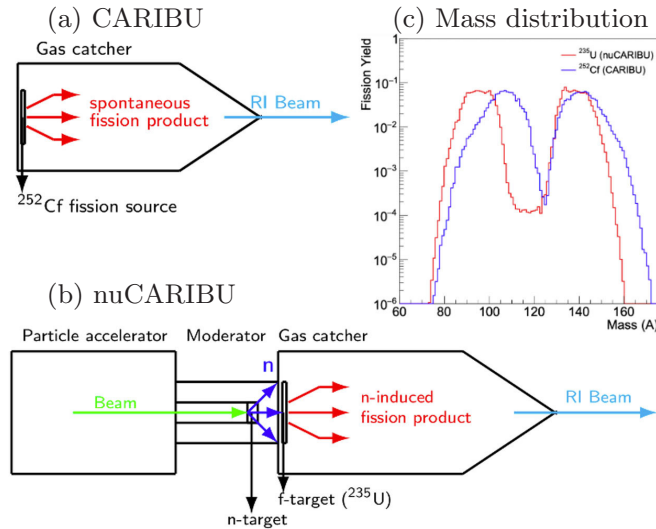


FIG. 1. Schematic layouts of CARIBU (a) and nuCARIBU (b). Comparison of the mass distribution for the spontaneous fission products for ^{252}Cf and the neutron induced fission for ^{235}U (c).

single-particle transfer around doubly magic ^{132}Sn , since the thermal neutron induced fission source would produce about 4 times more yield per fission. The nuCARIBU beam source consists of two targets (neutron production and fission target), a low-energy proton particle accelerator, a moderator and the existing CARIBU gas catcher. The neutrons generated via proton-induced reactions on a lithium target are thermalized by passing through a moderator. The resulting thermal neutrons produce fission products on a thin ^{235}U foil located inside the gas catcher. The fission products are thermalized in the gas catcher and then extracted, mass separated, and delivered to experiments with or without further acceleration. In developing the nuCARIBU concept, it was found via Monte Carlo simulations using the PHITS code [13] that a neutron generator [14,15] based on the $^7\text{Li}(p, n)$ reaction combined with a $(\text{C}_2\text{H}_4)_n$ moderator should provide the desired fission yields (see Sec. 2 in the Appendix). In the simulation study, the fission rate of nuCARIBU is predicted to be $\approx 9 \times 10^8$ fission per seconds in the ^{235}U foil, which is 18 times higher than that of the current CARIBU.

Before proceeding with the construction of nuCARIBU, it was considered prudent to confirm the Monte Carlo simulations [16] on which our design is based. The nuCARIBU validation experiments were performed for the $p - ^7\text{Li}$ option using a simplified geometry of the $(\text{C}_2\text{H}_4)_n$ moderator with a 4 MeV proton beam to measure the fission per proton compared with the predictions of the simulation. Two versions of the simplified geometry were simulated and tested experimentally. The first used four sheets (3.81 cm total thickness) of $(\text{C}_2\text{H}_4)_n$ between the LiF target and the ^{235}U foil, and the second used two sheets (1.91 cm thickness). These simulations tested two different degrees of moderation.

II. SIMULATION

The simplified geometry illustrated in Fig. 2 was used for the validation experiment. The setup was comprised of the

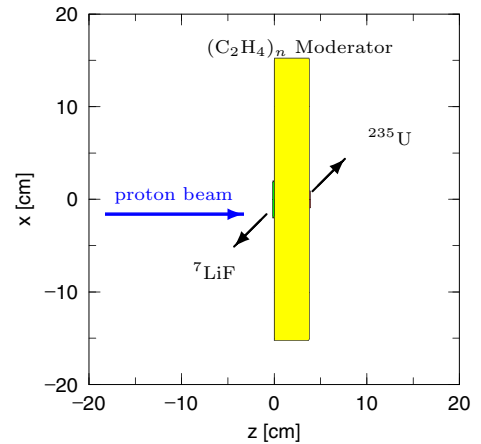


FIG. 2. Geometry for simulations.

LiF neutron production target, the $(\text{C}_2\text{H}_4)_n$ moderator and the ^{235}U fission foil. A monoenergetic 4 MeV proton beam with full width at half-maximum (FWHM) of 4 mm was delivered to the target by the ATLAS accelerator. The detailed input parameters for the simulation are tabulated in Table I. All simulations were done using the PHITS code, which is a Monte Carlo particle and heavy ion transport simulation code. Neutron production at the LiF target was simulated with user defined cross section data using well-known double differential cross sections [17]. For the neutron transport through the moderator material, the ENDF/B-VI.8 library for the kernel was used. The moderator temperature was fixed at room temperature (296 K). Lastly, the $^{235}\text{U}(n, f)$ cross sections in the JENDL 4.0 library [18] were used to produce fission products in the fission foil.

TABLE I. Input parameters for the simulation.

Projectile	
Beam	proton
Energy (MeV)	4
Beam current (μA)	0.16
Gaussian beam (FWHM in mm)	4
n -production target	
Target	LiF ($^{\text{nat}}\text{Li}$; 92.4% ^7Li)
Density (g/cm^3)	1.5
Thickness (mm)	2
Diameter ($\text{cm}\phi$)	1.3
Moderator	
Material	$(\text{C}_2\text{H}_4)_n$
Density (g/cm^3)	0.98
Area (cm^2)	30.5×30.5
Thickness (cm)	3.81 & 1.91
Fission target	
Target	^{235}U
Density (g/cm^3)	18.3
Thickness (mg/cm^2)	369
Diameter ($\text{cm}\phi$)	2

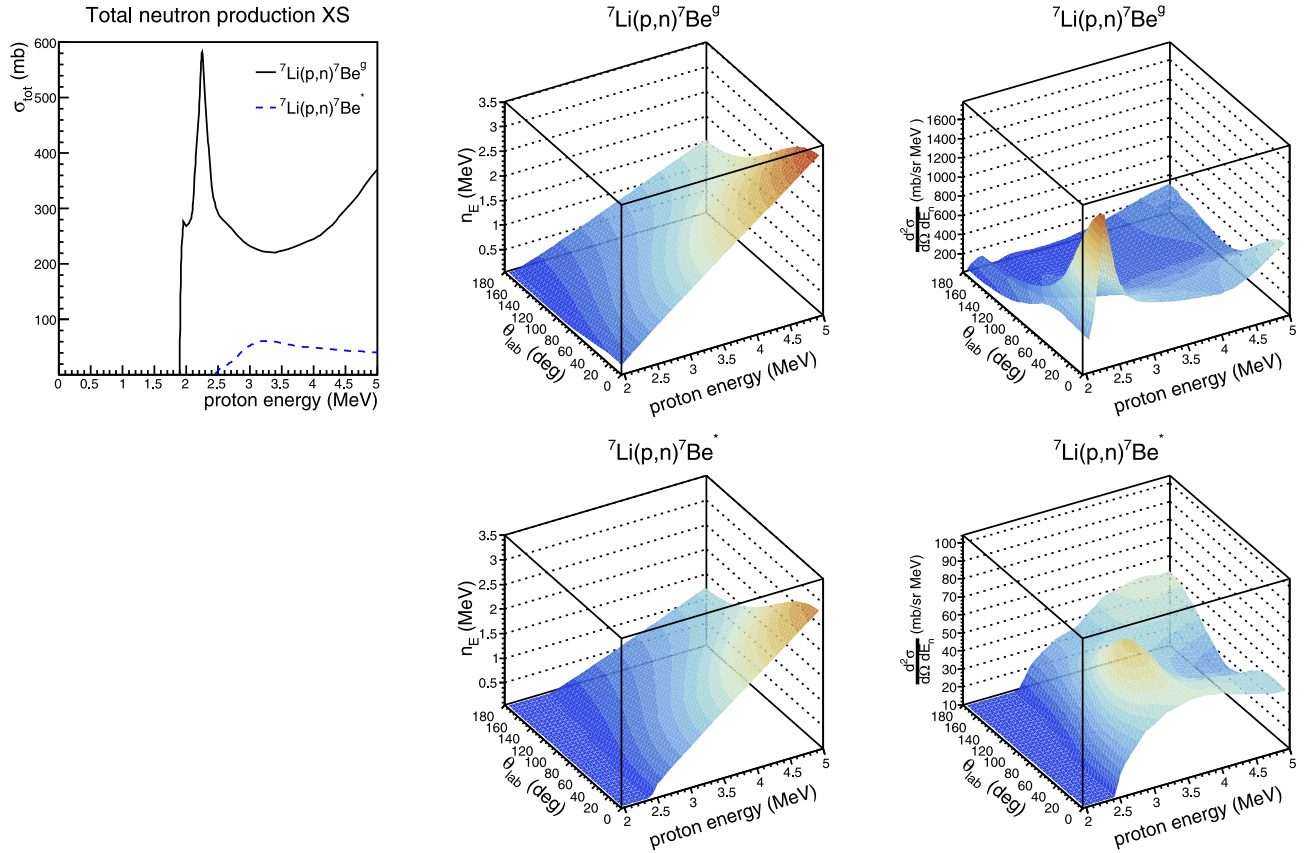


FIG. 3. Total neutron production cross section vs proton energy (left), emitted neutron energies (middle), and double differential cross sections (right) as functions of the laboratory incident proton energy and neutron emission angle for the reactions of ${}^7\text{Li}(p, n){}^7\text{Be}^g$ (upper) and ${}^7\text{Li}(p, n){}^7\text{Be}^*$ (lower). Data were taken from [17]. Here, XS stands for cross section.

A. Neutron production cross sections

The double differential cross sections from the evaluated data base [17] for the ${}^7\text{Li}(p, n)$ cross sections to the ${}^7\text{Be}$ ground and first excited states were input to PHITS for these simulations. Figure 3 illustrates the total neutron production cross section, angular dependence of emitted neutron energy and double differential cross section, $\frac{d^2\sigma_n}{d\Omega dE_n}$, in the laboratory frame from threshold energy to 5 MeV.

B. Neutron scattering kernel

The energy and angular distribution of outgoing neutrons in the moderator can be simulated using the evaluated neutron scattering library. PHITS used the neutron scattering kernel of the ENDF/B-VI.8 library. The $(\text{C}_2\text{H}_4)_n$ material, the moderator for the simulation, was evaluated based on a classical molecular dynamics model [19]. The kernel for room temperature $(\text{C}_2\text{H}_4)_n$ was used in these simulations.

C. Neutron energy distribution

The fast neutrons produced in the LiF target via the ${}^7\text{Li}(p, n)$ were moderated in the $(\text{C}_2\text{H}_4)_n$. The moderated neutron energy distribution at the fission target was calculated with the libraries above. Figure 4 shows the neutron-induced

fission total cross section vs energy for ${}^{235}\text{U}$ and the simulated moderated neutron flux vs energy at the ${}^{235}\text{U}$ foil for the two thicknesses of $(\text{C}_2\text{H}_4)_n$ that were used. The increase of thermal neutron flux is important as the fission cross section is inversely proportional to neutron velocity. The simulated fission product yields included contributions from the simulated

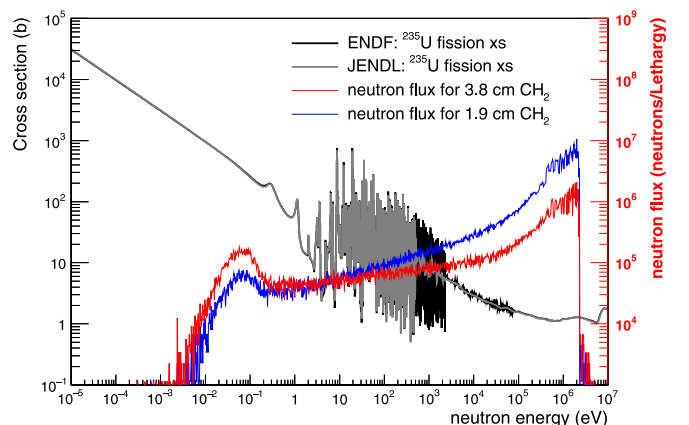


FIG. 4. Simulated neutron flux energy spectrum at the ${}^{235}\text{U}$ fission target compared with the neutron-induced fission cross section.

TABLE II. Simulated fission rates for various thicknesses of $(C_2H_4)_n$ moderator.

Moderator thickness (cm)	fission rate $\times 10^5$	uncertainty (%)
0.9525	0.84	7
1.905	1.00	3
2.8575	1.20	6
3.810	1.51	2
4.7625	1.44	5

neutrons for all energies shown in Fig. 4, but the yields are dominated by the large cross sections at the thermal energies. The thermal neutron flux for the 3.81 cm thick moderator case was three times higher than for the other thickness, whereas the epithermal and fast neutrons were reduced by a similar factor. The fission yields were given by the product of the cross section and flux at each energy. For example, the fission yield at the thermal “bump” below 0.1 eV is about 27 times the yield from the fast neutron “bump” at ≈ 1 MeV for the 3.81 cm thick moderator.

D. Fission rate

Fission rates in the ^{235}U foil for several moderator thicknesses were obtained by PHITS simulations based on JENDL-4.0 and the statistical uncertainties based on the number of Monte Carlo protons were simulated to be $\approx 3\%$ for the two selected cases (3.81 and 1.91 cm thick moderators), while other cases were calculated to be $\approx 5\text{--}7\%$ (see Table II). Simulations were performed with $10^9\text{--}10^{10}$ protons, depending on the case. The PHITS simulations were run on the Argonne computer cluster Bebop. The total mass and enrichment of the ^{235}U fission foil were 1.16 g and 97.8%, respectively. The 3.81 and 1.91 cm thicknesses of $(C_2H_4)_n$ moderator for the experiments were chosen based on the simulation with the former giving near the peak of the simulated fission rate, while the thinner was predicted to yield $\approx 2/3$ of that. The fission rates for the 3.81 and 1.91 cm were predicted to be 1.51×10^5 and 1.00×10^5 f/s, respectively. The γ -ray intensities from the fission products were predicted with the post-processor DCHAIN (simulation code for calculating the time dependence of activation during and after irradiations). We used these simulation results to decide the proton beam current, irradiation time, and measurement time for the experiments. The expected radioactivities from decay of selected fission nuclei (see Sec. III) and their daughter nuclei after 1 h irradiation are displayed in Fig. 5. Solid lines indicate selected isotopes.

III. METHOD

The fission rate of ^{235}U can be determined by counting β -delayed γ rays from decay of fission products. γ rays from ^{92}Sr (1383.93 keV), ^{104}Tc (358 keV), ^{134}Te (565.992 keV), and ^{138}Xe (258.411 keV) were selected based on several requirements: 1) relatively short half-life and high cumulative fission yield to obtain enough statistics, 2) short half-life of the parent nuclei of selected nuclei to use cumulative fission yield, 3) non-overlapping γ peak to avoid γ ray feeding from

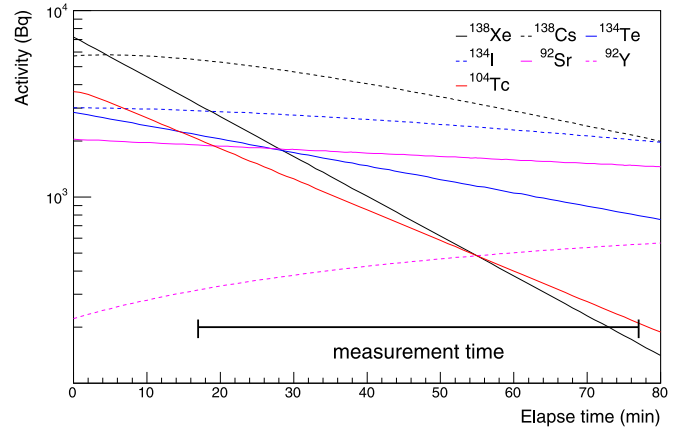
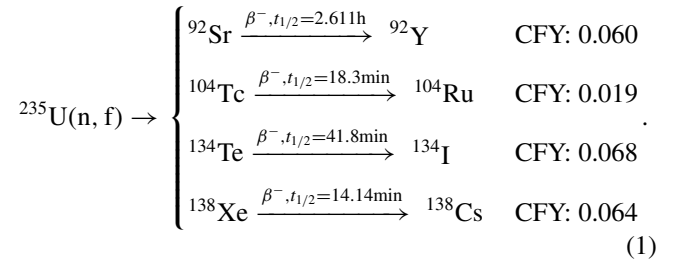


FIG. 5. Radioactivities for selected nuclei as a function of elapsed time after EOB. The bottom bar indicates the gamma measurement time beginning 17 minutes after EOB. Simulations were done with the DCHAIN code.

decay of the other nuclei. The following are the half-lives and cumulative fission yields (CFY) of the four selected fission products in thermal-neutron induced fission:



The CFY includes the probability of the direct production of the isotopes and the cumulative yields from the decays of more neutron-rich isobars [20]. In this experiment, γ rays emitted from selected fission products were detected at a delay time of ≈ 20 min (due to the safety survey) after ≈ 1 h irradiation. Most of the parent nuclei with short half-life (most are few seconds except for $^{104}\text{Mo} \rightarrow ^{104}\text{Tc} \approx 1$ min) had decayed away. The selected fission products were no longer produced via the decay of their parents. In this case, the fission rate of ^{235}U was obtained approximately by using the equation of radioactive growth and decay:

$$\begin{aligned} N_{\text{evt}} &= N_{\text{obs}} \cdot C_{\epsilon} \cdot C_{\text{sab}} \cdot C_{\gamma-br} \cdot C_{DT} \\ &= \frac{R}{\lambda} \underbrace{(1 - e^{-\lambda t_{ir}})}_{\text{irradiation}} \underbrace{e^{-\lambda t_c}}_{\text{cool down}} \underbrace{(1 - e^{-\lambda \Delta t})}_{\text{measurement}}, \\ R_f &= R / \text{CFY}, \end{aligned} \quad (2)$$

where R_f stands for the fission rate of ^{235}U , R is the production rate of each nucleus, and N_{evt} is the total number of events for selected nuclei. N_{obs} is the observed γ -ray counts by the high purity germanium (HPGe) detector, C_{ϵ} , C_{sab} , $C_{\gamma-br}$, and C_{DT} are corrections for detector efficiency, γ -ray self-absorption by passing through the fission target, γ -ray branching ratio, and detector dead time during measurements, respectively. The C_{DT} is 1.0256 for a typical 2.5% dead time in these

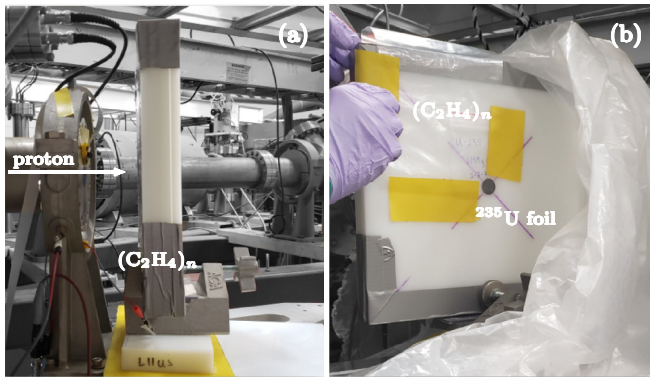


FIG. 6. Experimental setup of this experiments with 3.81 and 1.91 cm thick $(C_2H_4)_n$ moderators. LiF neutron production target, and the enriched ^{235}U fission foil were attached in front of and behind $(C_2H_4)_n$ moderator plates. (a) Side view and real picture of the schematic view in Fig. 2. (b) Back side view showing ^{235}U foil.

measurements. λ is the decay constant. Irradiation time, cooling time and measurement time are expressed as t_{ir} , t_c , and Δt , respectively.

IV. EXPERIMENTAL

Experiments were carried out at ATLAS using an experimental setup placed in the air as shown in Fig. 6. A natural LiF (92.4% 7Li) neutron production target (1.3 cm diameter and 2 mm thick) and 97.8% enriched ^{235}U fission foil (2.0 cm diameter and 0.2 mm thick) were mounted on front and rear sides of a 30.5 cm \times 30.5 cm \times 3.81 cm $(C_2H_4)_n$ moderator plate, respectively. The 4 MeV, 0.16 μA proton beam impinged on the neutron production target (LiF) to produce neutrons via the $^7Li(p, n)$ reaction. The produced neutrons were moderated by passing through the $(C_2H_4)_n$ moderator. Fission products were generated in the fission ^{235}U foil by the neutron-induced reaction with these moderated neutrons. The enriched ^{235}U fission foil was irradiated approximately for 1 h. After irradiation, β -delayed γ rays from the fission products were counted with a portable HPGe detector placed 22 cm behind the fission foil. In order to test the PHITS simulation predictions vs moderator thickness, two irradiations with different thickness (3.81 cm and 1.91 cm) of $(C_2H_4)_n$ moderator were performed.

A. Proton beam

The linac output proton beam energy was 5.22 MeV and the final energy on the LiF target was 4 MeV after passing through a 25 μm thick Ti window and 5.5 cm of air, since the experimental setup was installed outside of vacuum. The beam current of 0.16 μA was measured by a suppressed Faraday cup in front of the Ti window before the experiment and monitored by a thin Al foil placed between the LiF target and $(C_2H_4)_n$ moderator during the irradiation. The beam was focused to be smaller than the diameter of the LiF target. The target (left) and beam spot on target (right) are shown in Fig. 7.

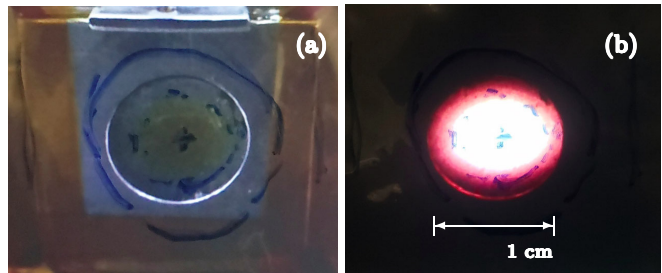


FIG. 7. The picture of beam on LiF target. (a) Picture of LiF target and (b) picture of fluorescent beam spot on LiF target.

B. Measurement

As described in Sec. III, the γ rays of 1383.93, 385.0, 565.992, and 258.411 keV from ^{92}Sr , ^{104}Tc , ^{134}Te , and ^{138}Xe were measured and analyzed after irradiation. The above nuclei are near the mass number 100 of the light mass peak regions and 134 of the heavy mass peak regions of the fission mass distribution. Decay data and detector absolute efficiency for the selected fission nuclei are summarized in Table III. Detailed γ spectra for 60 minute accumulation are shown in Sec. V.

1. Detector and dead time

After irradiation, γ -ray spectra were measured by a portable HPGe detector with a 50 mm \times 40 mm HPGe crystal at a distance of 22 cm from the ^{235}U fission target shown in Fig. 8. There is a systematic error of a few % from the uncertainty in the distance between the fission target and detector. During the measurements, the average dead time was 2.5% approximately.

2. Detector efficiency

The HPGe detector efficiency, shown in Fig. 9 was calibrated by a mixed radioactive calibration source at a distance of 25 cm. The efficiency for the selected γ rays was calculated by the following formula [23]:

$$\epsilon = e^{[(A+Bx+Cx^2)^{-G} + (D+Ey+Fy^2)^{-G} - (-G)]^{-1/G}}, \quad (3)$$

where x and y are $\ln(E_\gamma/100)$ and $\ln(E_\gamma/1000)$, respectively. E_γ is the γ -ray energy of interest in keV. The uncertainty in the detector absolute efficiency is less than 2%. The constants A – G were determined by a fit to the measured γ efficiencies. The discrepancies between the fitted and measured values are

TABLE III. Decay and detector efficiency information for the selected isotopes. Data were taken from National Nuclear Data Center (NNDC) and Idaho National Laboratory Gamma-ray Spectrometry Catalog [21,22].

nucl.	half-life	γ peak (keV)	branch ratio (%)	det eff $\times 10^{-4}$
^{92}Sr	2.611 h	1383.93	90 (6)	1.49
^{104}Tc	18.3 min	358.0	89 (3)	6.03
^{134}Te	41.8 min	565.992	18.6 (10)	3.61
^{138}Xe	14.14 min	258.411	34.1 (13)	8.73



FIG. 8. The picture of γ -ray peak measurement with portable HPGe detector. The distance from ^{235}U target to the detector was 22 cm.

shown in the lower part of Fig. 9. The calibrated detector efficiency, corrected for the actual distance of 22 cm vs 25 cm, as a function of γ -ray energy for the selected nuclei are summarized in Table III.

3. Self-absorption

The thickness of the ^{235}U fission foil was 0.369 g/cm^2 . For low energy emitted γ in the high Z and high density ^{235}U foil, the self-absorption for escaping γ rays cannot be neglected. The correction factor of self-absorption can be calculated by

$$1/C_{\text{sab}} = \frac{\int_0^{x_0} \alpha(x) e^{-\mu(x_0-x)} dx}{\int_0^{x_0} \alpha(x) dx}, \quad (4)$$

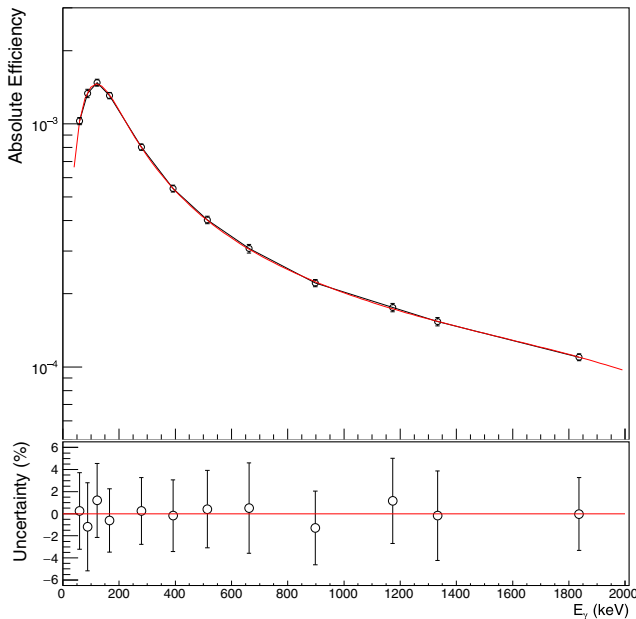


FIG. 9. Absolute HPGe detector efficiency at a distance of 25 cm and its uncertainty as a function of γ energy from the mixed calibration source.

where μ stands for the mass attenuation coefficients which were taken from the NIST database [24]. The x_0 is the total thickness of the fission target and the $\alpha(x)$ is the activity density. In these experiments, the activity density was taken to be linear with respect to thickness, $\alpha(x) = 1 - ax$, based on the PHITS simulations. This correction factor was used to calculate the self-attenuation of γ intensity by passing through the full thickness of the fission target.

C. Subtraction of γ rays from the residual products

The simulations and measurements were carried out using two different thicknesses of $(\text{C}_2\text{H}_4)_n$ moderator. Initially, the experiment was conducted using a thick moderator to obtain measurements. Subsequently, two moderator slabs were removed, and the experiment was repeated with a thin moderator after a 114 min interval. Due to the reuse of the ^{235}U target, the residual activity in the fission target was subtracted. For the second run (1.91 cm thick moderator), the observed γ rays were determined by subtracting the γ rays from the residual fission nuclei from the first run. The expected γ rays from the decay of the residual activity from the first run can be determined by

$$\begin{aligned} N_{\text{obs}} \cdot C_{\text{all}} &= \frac{R}{\lambda} (1 - e^{-\lambda t_{\text{ir}}}) e^{-\lambda t_c} (1 - e^{-\lambda \Delta t}), \\ N'_{\text{obs}} \cdot C_{\text{all}} &= \frac{R}{\lambda} (1 - e^{-\lambda t'_{\text{ir}}}) e^{-\lambda t'_c} (1 - e^{-\lambda \Delta t}), \\ N'_{\text{obs}} &= N_{\text{obs}} \cdot \frac{e^{-\lambda t'_c}}{e^{-\lambda t_c}}, \end{aligned} \quad (5)$$

where N'_{obs} stands for the expected γ count during the second measurements. t'_c is the new cooling time before the second run measurement. The expected γ counts were calculated by multiplying the observed γ counts in the first run by the ratio of cooling terms.

V. RESULTS

Comparison of γ spectra for the two cases accumulated for 60 min from ≈ 20 min after the end of bombardment is presented in Fig. 10. The emitted γ energies of 1383.93, 358.0, 565.992, and 258.411 keV were selected to identify the fission products. The total absolute number of detected γ rays in the peaks, N_{obs} , was analyzed and used to determine the fission yield during the irradiation. The whole spectra can be found in Fig. 10. As shown in Sec. III, the fission rate from the total number of detected γ rays, N_{obs} , was calculated by

$$R_f = R/CFY = \frac{C_{\text{all}} \cdot \lambda \cdot N_{\text{obs}}}{(1 - e^{-\lambda t_{\text{ir}}}) e^{-\lambda t_c} (1 - e^{-\lambda \Delta t})} / CFY. \quad (6)$$

The ratios of experiments and simulation were determined by the cumulative fission yield using the JEFF [25] and JENDL databases. The integration time for ^{92}Sr and ^{134}Te was 60 min, however the time for ^{104}Tc and ^{138}Xe was 40 min due to their shorter half-lives. The statistical error was calculated by RADWARE [23] and total error includes systematic errors. Here, a 2% uncertainty in the detector efficiency and a few % uncertainty in the γ -ray branching ratios for the selected nuclei were included to calculate the systematic error. The

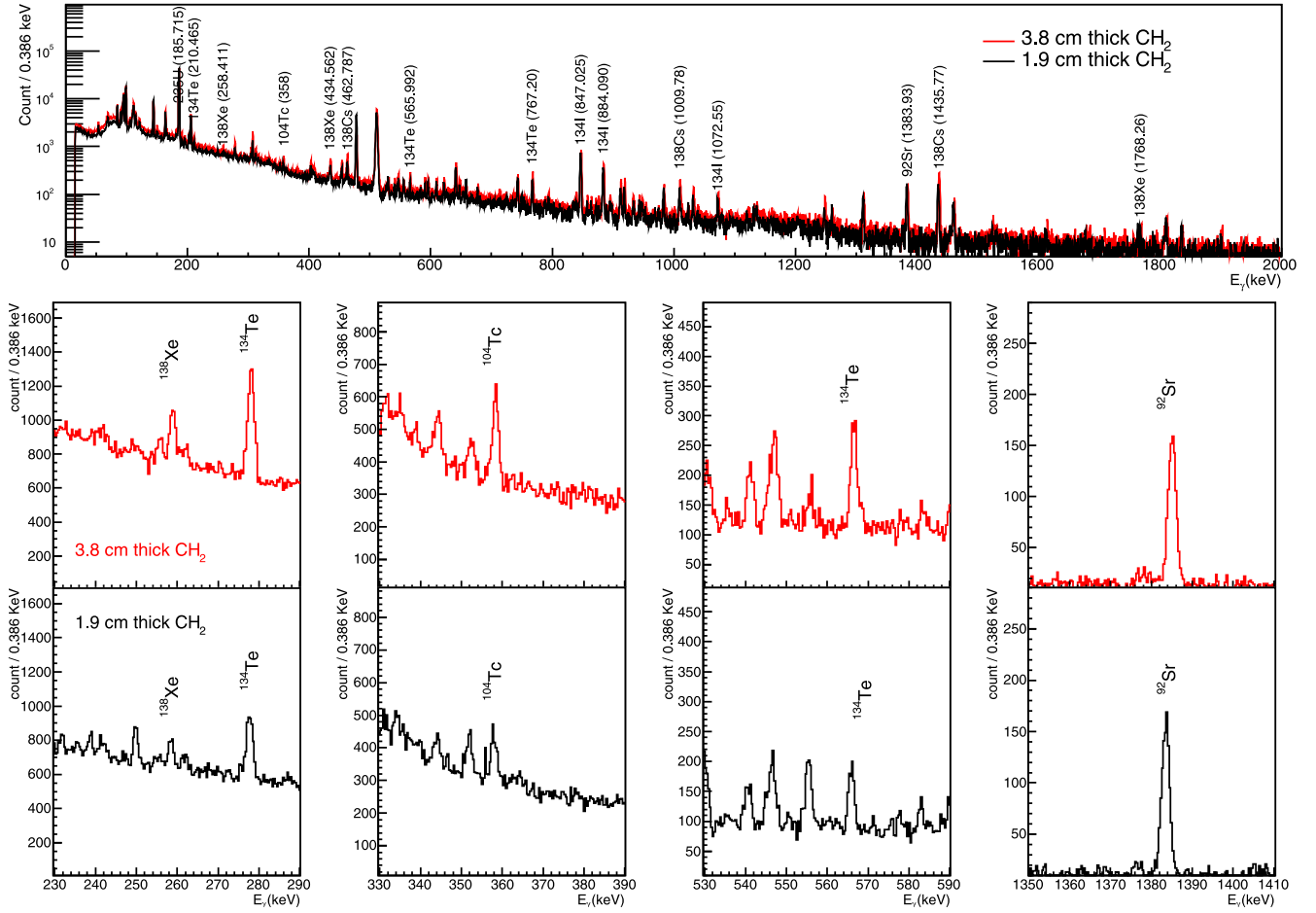


FIG. 10. Comparison of γ ray spectra from the decay of ^{235}U fission products in moderator cases with thicknesses of 3.8 cm and 1.9 cm. Spectra were accumulated over a 1 h. The spectrum for the 1.9 cm case includes γ rays from residual nuclei, as the ^{235}U target was reused.

total error was obtained by

$$\Delta R_f^{\text{total}} = R_f \sqrt{\left(\frac{\Delta N_{\text{obs}}}{N_{\text{obs}}}\right)^2 + \left(\frac{\Delta \epsilon_0}{\epsilon}\right)^2 + \left(\frac{\Delta I_{\gamma-br}}{I_{\gamma-br}}\right)^2}, \quad (7)$$

where N_{obs} , ϵ , and $I_{\gamma-br}$ are the number of the detected γ rays, detector efficiency, and γ -ray branching ratio, respectively. The simulated moderated neutron flux vs energy is shown in Fig. 4, so the modified CFY with the weight of the thermal and fast neutron is needed to determine the fission rate. The fission yield ratios at the thermal and fast neutron energy for the 3.81 cm and 1.91 cm $(\text{C}_2\text{H}_4)_n$ cases are 27 and 2.5, respectively. With these ratios, the weighted CFYs were calculated. The fission rates determined using the weighted CFYs are tabulated in Table IV. The effect of the weighted fission rate compared to the thermal fission rate is randomly $\approx \pm(1-6)\%$. The cumulative fission yield for the ^{235}U fission products varied slightly between the libraries. There is a few percent variation of cumulative fission yield depending on the neutron energy. The cumulative fission yield induced by thermal and fast neutrons in the literature are listed in Table V. PHITS applied the energy dependent CFY case by case depending on neutron energy.

A. Ratio of fission rates

The fission rates were determined in the above section. In order to verify the simulations, measured ^{235}U fission rates were compared with PHITS simulations obtained based on JENDL library. The ratio of experiments and simulations determined for the selected nuclei for both 3.81 cm and 1.91 cm thick $(\text{C}_2\text{H}_4)_n$ moderator cases are illustrated in Fig. 11. The measured fission rates on the figure were calculated with the thermal induced cumulative fission yield from JEFF library data. The blue line shows the normalized fission rates of simulations with statistical errors, $\approx 2\%$. The ratio of fission rates between experiments and simulations are calculated by the constant fit with the ratios of four selected nuclei. The red dotted lines are the fit results shown in Fig. 11. The fit ratios between the experiments and simulations for the 3.81 cm and 1.91 cm $(\text{C}_2\text{H}_4)_n$ cases are 1.039(35) and 0.928(54), respectively.

VI. CONCLUSION AND DISCUSSION

The nuCARIBU simulation validation experiments on enriched ^{235}U fission target bombarded by the thermal neutrons produced via the reaction of $^7\text{Li}(p, n)$ were performed using

TABLE IV. Fission rates for two moderator thicknesses. The symbol “w-” indicates the weighted values.

nucl.	N_{obs}	N_{evt}	R	FR JEFF	w-FR JEFF	FR JENDL	w-FR JENDL	ratio JEFF	w-ratio JEFF	ratio JENDL	w-ratio JENDL	stat. err (%)	tot. err (%)
	3.81 cm	thick $\times 10^6$	moderator $\times 10^3$	$\times 10^5$	$\times 10^5$	$\times 10^5$	$\times 10^5$						
^{92}Sr	981	5.87	8.60	1.43	1.43	1.45	1.45	0.943	0.959	0.959	0.944	3.3	7.1
^{104}Tc	1061	1.68	3.12	1.66	1.65	1.66	1.65	1.098	1.096	1.092	1.090	5.8	6.8
^{134}Te	931	11.34	10.81	1.59	1.60	1.55	1.55	1.053	1.026	1.028	1.060	5.1	5.5
^{138}Xe	1325	4.06	10.33	1.61	1.62	1.64	1.65	1.067	1.087	1.089	1.070	14.0	14.2
	1.91 cm	thick $\times 10^6$	moderator $\times 10^3$	$\times 10^5$	$\times 10^5$	$\times 10^5$	$\times 10^5$						
^{92}Sr	529	3.15	5.85	0.97	0.98	0.99	0.99	0.970	0.987	0.991	0.978	7.5	9.8
^{104}Tc	513	0.81	1.75	0.93	0.88	0.93	0.91	0.935	0.933	0.906	0.878	10.0	10.6
^{134}Te	439	5.35	6.20	0.91	0.97	0.89	0.91	0.914	0.891	0.906	0.966	9.6	9.9
^{138}Xe	672	1.92	5.54	0.86	0.88	0.88	0.89	0.865	0.882	0.894	0.884	13.4	13.6

the activation method at Argonne. During the experiments, two moderator cases (3.81 cm and 1.91 cm thickness) were carried out. The 1383.93 keV (^{92}Sr), 358.0 keV (^{104}Tc), 565.992 keV (^{134}Te), and 258.411 keV (^{138}Xe) γ rays were selected and analyzed to calculate production rates for each fission product. Measured fission rates were compared with PHITS simulation results based on JENDL library. The observed ratios from four different fission nuclei are consistent. For both the 3.81 cm and 1.91 cm thick moderator cases, good agreement within uncertainties between the simulated and the measured yields were observed. The experimental yields were 1.039(35) and 0.928(54) times the simulated yields, respectively. It is determined that the results of this validation experiment are adequate for launching the nuCARIBU project. The case that gives the best agreement is the one closest to the actual geometry to be used.

The nuCARIBU will provide a neutron-induced fission yield of $\approx(9.3 \pm 0.5) \times 10^8$ f/s in the ^{235}U foil by employing neutrons produced by a 5 MeV, 0.5 mA proton beam on a ^7Li target, far exceeding the fission yield of $\approx 5 \times 10^7$ f/s available with the current ^{252}Cf source of the CARIBU. The predicted fission product distributions for the neutron-induced fission of nuCARIBU are compared to the distributions for the spontaneous fission of CARIBU in Figure 12. The fission product distribution changes significantly from the distribution of the spontaneous fission source of ^{252}Cf . The fission

TABLE V. Thermal and fast (500 keV) neutron induced cumulative fission yield.

nucl.	JENDL		JEFF	
	thermal	fast	thermal	fast
^{92}Sr	0.059320	0.058389	0.060340	0.058614
^{104}Tc	0.018795	0.020707	0.018759	0.022917
^{134}Te	0.069659	0.065588	0.067872	0.055331
^{138}Xe	0.062861	0.059955	0.064050	0.059348

yield is obviously reduced in the mass region, $106 < A < 120$ and $A > 154$ (see the bottom panel of Fig. 12(a)). On the other hand, the fission yield in the ^{132}Sn region ($120 < A < 154$) and in the ^{78}Ni region ($A < 106$) will be considerably increased with nuCARIBU. As shown in Fig. 12(b), the estimated yield of ^{132}Sn for nuCARIBU is ≈ 80 times higher than for CARIBU. This is well suited to the coming single-particle transfer reaction programs with HELIOS [26]. These results provide strong support for the neutron-induced ^{235}U fission source approach of nuCARIBU to replace the existing ^{252}Cf source.

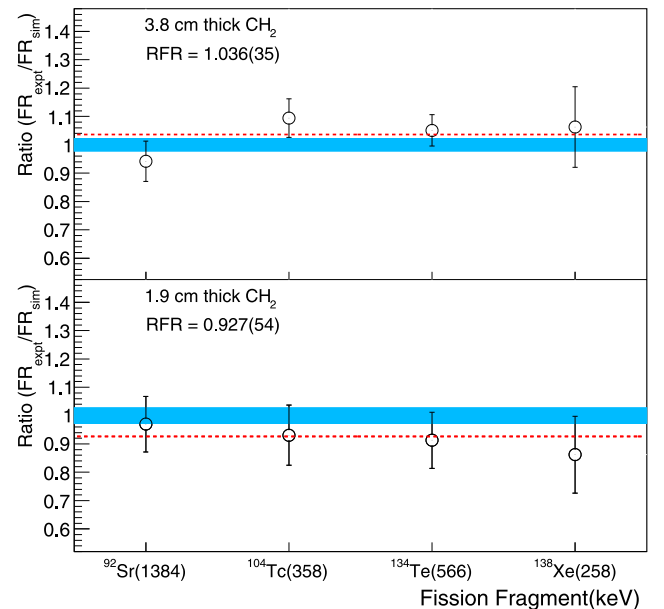


FIG. 11. Comparison of fission rates between measurements and simulations. RFR indicates the ratio of fission rates between experiments and simulations.

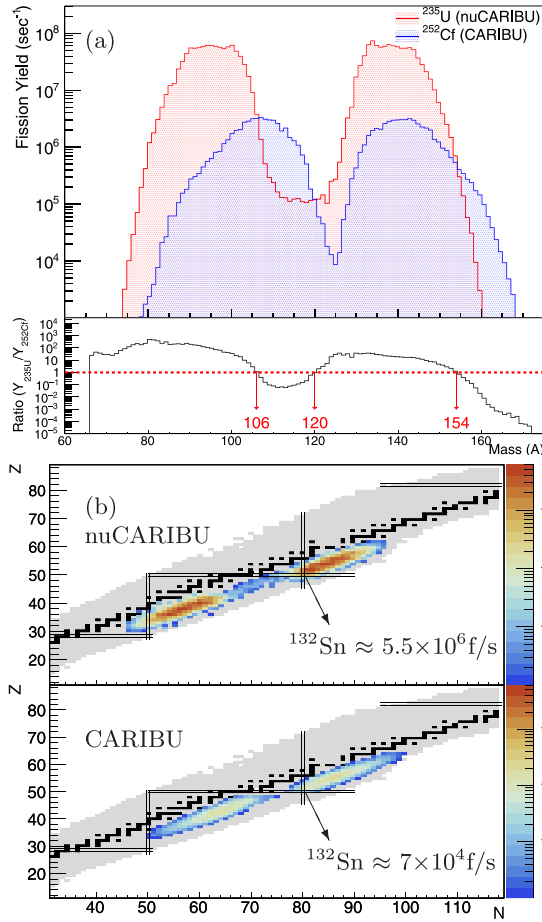


FIG. 12. (a) Fission fragment yields by mass for thermal neutron induced fission of ^{235}U (nuCARIBU) and spontaneous fission of ^{252}Cf (CARIBU). (b) Fission fragment distributions for nuCARIBU (upper) and CARIBU (lower).

ACKNOWLEDGMENTS

The authors would like to thank the ATLAS operators and staff for their help during the experiments. We gratefully acknowledge the computing resources provided for use of Bebop, a high-performance computing cluster operated by the Laboratory Computing Resource Center at Argonne National Laboratory. This work was supported by the U.S. Department of Energy, Office of Nuclear Physics, under Contract No. DE-AC02-06CH11357. This research used resources of ANL's ATLAS facility, which is a DOE Office of Science User Facility.

APPENDIX: NEUTRON GENERATOR SIMULATION

The simulations performed using the PHITS code present the results of a feasibility study focused on transitioning from CARIBU to nuCARIBU. This study aims to establish an appropriate nuCARIBU concept to enhance fission product yield. Initial comparative simulations were performed between DD and $p - ^7\text{Li}$ reactions. Subsequently, a selection of moderator materials from $(\text{C}_2\text{H}_4)_n$, H_2O , D_2O , and Be

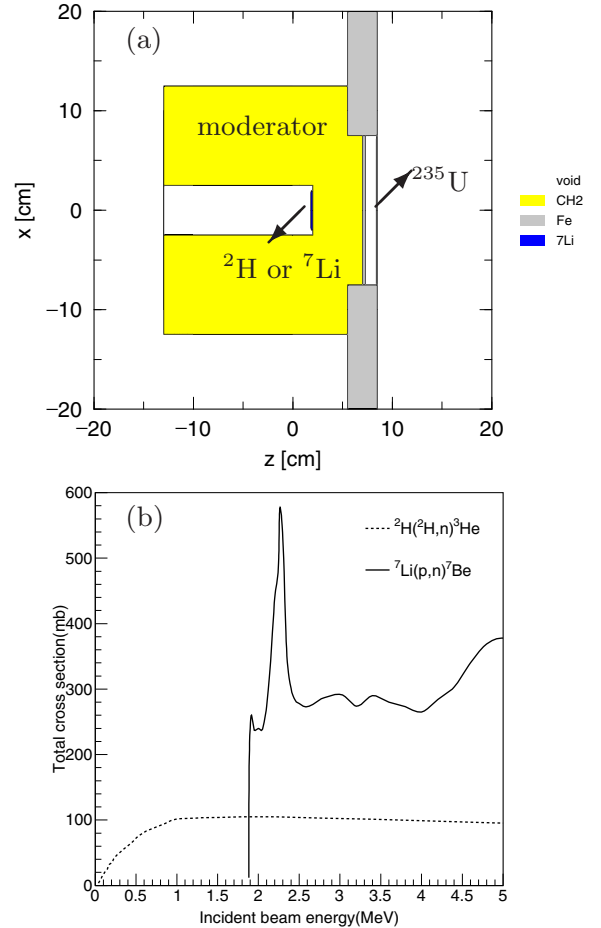


FIG. 13. (a) Geometry of nuCARIBU target assembly in the simulations. The beam comes in from the left. (b) Total neutron production cross sections for the DD (dotted line) and $p - ^7\text{Li}$ (solid line) reactions as a function of incident beam energy.

was undertaken. Finally, the selected reaction and moderator material were employed to optimize the geometry.

Note that the inputs used for these simulations to define the nuCARIBU concept are different from those used for the validation test simulation in Sec. II. For instance, in these simulations, we utilized an ideal ^7Li target (not LiF), and various parameters such as beam energy, target thickness, and moderator thickness were varied.

1. Inputs and target system

There are many ways to produce thermal neutrons using low energy accelerators. In this study, DD and $p - ^7\text{Li}$ reactions were considered. In order to compare these methods, we simulated thermal neutron fluxes (< 10 eV) produced by the reactions of $^2\text{H}(d, n)^3\text{He}$ and $^7\text{Li}(p, n)^7\text{Be}$ with the setup shown in Fig. 13(a). 0.3 and 3 MeV deuteron beams and 3 MeV proton beam were used and incident beam parameters and physical properties of target are summarized in Table VI. For the $p - ^7\text{Li}$ option, it is effective to use a proton beam with energy above 2.3 MeV because of the relatively high cross section near the reaction resonance (see Fig. 13(b)).

TABLE VI. Initial beam parameters and physical properties of targets.

Projectile	Energy MeV	current mA	diameter mm ϕ
d	0.3, 3	0.25	10
p	3	0.25	10
neutron target	density g/cm ³	thickness mm	diameter mm ϕ
² H	1	2	20
⁷ Li	0.534	2	20
fission target	density g/cm ³	thickness mg/cm ²	diameter mm ϕ
²³⁵ U	19.1	5	100

2. Neutron generator options

Figure 14 shows thermal neutron fluxes with energy below 10 eV on the target system for *DD* and $p - ^7\text{Li}$ generators, which are plotted on the same scale for z . As can be seen, the $p - ^7\text{Li}$ option is a more efficient way to produce thermal neutron than the *DD* option. The total neutron yields per projectile on the fission target are 5.5×10^{-9} (*DD* at 0.3 MeV), 1.1×10^{-6} (*DD* at 3 MeV), and 5.8×10^{-6} ($p - ^7\text{Li}$ at 3 MeV). According to these results, the $p - ^7\text{Li}$ neutron generator can produce more thermal neutrons by a factor of 5 compared to the *DD* neutron generator at 3 MeV per projectile. The $p - ^7\text{Li}$ neutrons are more forward focused and of lower initial energy so that this allows them to be thermalized more easily in a small volume which therefore leads to a higher flux per cm² out the ²³⁵U foil. The *DD* at 0.3 MeV produces roughly 200 times less thermal neutrons per incident projectile but this lower beam energy can be reached with electrostatic accelerators that can reach in some cases very high currents.

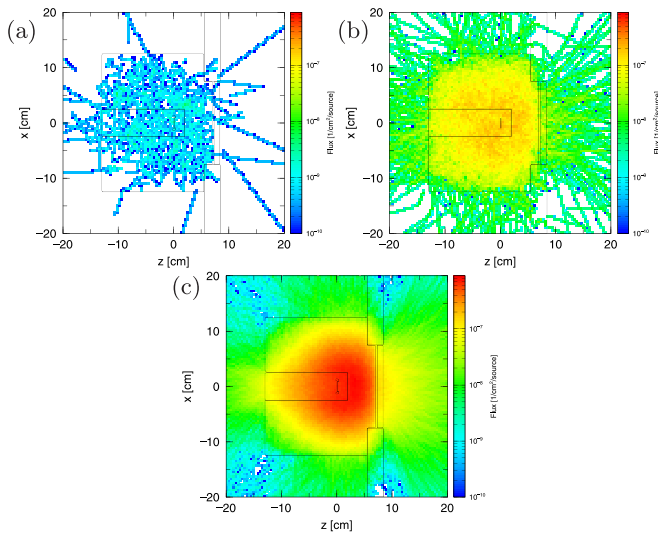


FIG. 14. Comparison of neutron fluxes ($E_n < 10$ eV) per projectile with a same H_2O moderator for the *DD* at 0.3 MeV (a), *DD* at 3 MeV (b), and $p - ^7\text{Li}$ at 3 MeV (c) generator options.

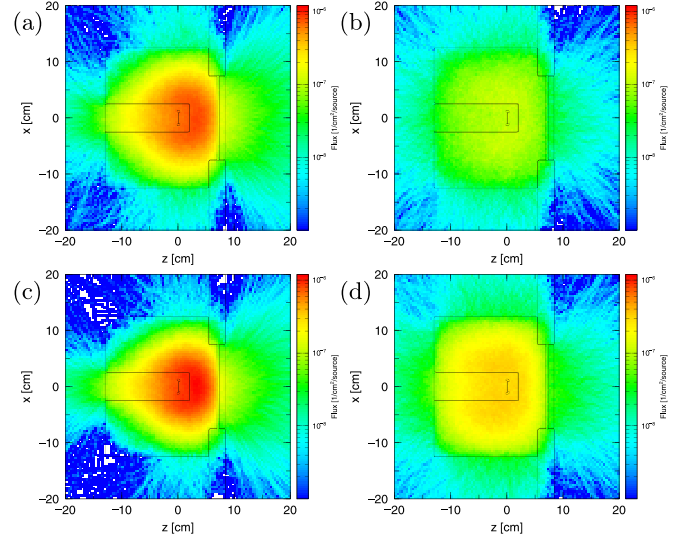


FIG. 15. Comparison of neutron fluxes ($E_n < 10$ eV) per projectile for H_2O (a), D_2O (b), $(\text{C}_2\text{H}_4)_n$ (c), and Be (d) moderator materials.

3. Optimization of the moderator material

As shown above, the $p - ^7\text{Li}$ neutron generator appears to have the highest yield as a neutron source. To determine which type of moderator is the most suitable to reduce neutron energies and improve thermal neutron intensity, simulations were performed using water, D_2O , $(\text{C}_2\text{H}_4)_n$, and Be as moderator materials. The simulated thermal neutron distributions for the four moderator materials are shown in Fig. 15. The neutron flux distributions for water and $(\text{C}_2\text{H}_4)_n$ are relatively narrow, in contrast neutrons moderated by D_2O and Be show much

TABLE VII. Thermal neutron intensities and fission rates on 10 cm ϕ target at the current of 0.5 mA. The mod. th. indicate moderator thickness.

		neutron flux $E_n < 10$ eV				
mod. th.	E_p (MeV)					
cm	2.5	3.0	3.5	4.0	5.0	
	$\times 10^{10}$	$\times 10^{10}$	$\times 10^{10}$	$\times 10^{10}$	$\times 10^{10}$	
1	2.2	3.4	4.4	5.4	8.2	
2	3.1	4.8	6.3	7.6	11.4	
3	3.5	5.5	7.3	8.8	12.6	
4	3.4	5.4	7.4	9.0	12.3	
5	2.8	4.9	6.6	8.1	10.2	
		fission rate				
mod. th.	E_p (MeV)					
cm	2.5	3.0	3.5	4.0	5.0	
	$\times 10^8$	$\times 10^8$	$\times 10^8$	$\times 10^8$	$\times 10^8$	
1	1.3	2.1	3.3	3.7	6.4	
2	2.0	3.4	5.2	4.8	8.5	
3	2.6	4.2	5.0	6.3	9.3	
4	2.5	4.0	5.2	7.0	9.0	
5	2.2	3.1	4.3	6.8	6.9	

broader distributions. Both water and $(\text{C}_2\text{H}_4)_n$ are good material as a moderator. However, comparing peak thermal neutron fluxes on the moderators, neutron intensity using $(\text{C}_2\text{H}_4)_n$ moderator is 20% higher which makes it the best choice of the four for $p - {}^7\text{Li}$.

4. Optimization of the thickness of the moderator

$(\text{C}_2\text{H}_4)_n$ was selected as the moderator material for these simulations. To optimize the thickness of the moderator, several simulations with moderator thicknesses from 1 to 5 cm and proton energies from 2.5 to 5 MeV were

performed to obtain the thermal neutron intensities on the fission target. The beam current was fixed at 0.5 mA. The calculated neutron intensities and fission rates are given in Table VII. Statistical errors of the neutron intensities and fission rates are $\approx 1\%$ and $\approx 5\%$, respectively. The moderated neutron intensity in the fission target increases with increasing proton beam energy at a fixed current. As the results, simulations show that maximum moderated neutron intensities are 3.5×10^{10} , 5.5×10^{10} , 7.4×10^{10} , 9.0×10^{10} , and 12.6×10^{10} neutrons/0.5 mA and the optimal thicknesses of moderators are between 3.0–4.0 cm with the proton energies from 2.5 to 5 MeV. The maximum fission rate is $\approx 9.3 \times 10^8$ fissions/0.5 mA.

-
- [1] G. Savard, S. Baker, C. Davids, A. F. Levand, E. F. Moore, R. C. Pardo, R. Vondrasek, B. J. Zabransky, and G. Zinkann, *Nucl. Instrum. Methods Phys. Res. B* **266**, 4086 (2008).
- [2] G. Savard, R. C. Pardo, S. Baker, C. N. Davids, A. Levand, D. Peterson, D. G. Phillips, T. Sun, R. Vondrasek, B. J. Zabransky, and G. P. Zinkann, *Hyperfine Interact.* **199**, 301 (2011).
- [3] G. Savard, A. J. Kreiner, A. A. Valda, D. M. Minsky, H. R. Somacal, M. E. Debray, and P. Stolia, *Proc. Conf. ARIS* **6**, 010008 (2014).
- [4] J. Van Schelt, D. Lascar, G. Savard, J. A. Clark, P. F. Bertone, S. Caldwell, A. Chaudhuri, A. F. Levand, G. Li, G. E. Morgan, R. Orford, R. E. Segel, K. S. Sharma, and M. G. Sternberg, *Phys. Rev. Lett.* **111**, 061102 (2013).
- [5] A. J. Mitchell *et al.*, *Phys. Rev. C* **93**, 014306 (2016).
- [6] B. Bucher *et al.*, *Phys. Rev. Lett.* **118**, 152504 (2017).
- [7] D. J. Hartley *et al.*, *Phys. Rev. Lett.* **120**, 182502 (2018).
- [8] W. Witt, V. Werner, N. Pietralla, M. Albers, A. D. Ayangeakaa, B. Bucher, M. P. Carpenter, D. Cline, H. M. David, A. Hayes, C. Hoffman, R. V. F. Janssens, B. P. Kay, F. G. Kondev, W. Korten, T. Lauritsen, O. Moller, G. Rainovski, G. Savard, D. Seweryniak, J. Smith, R. Stegmann, S. Zhu, and C. Y. Wu, *Phys. Rev. C* **98**, 041302(R) (2018).
- [9] R. Orford, N. Vassh, J.A. Clark, G.C. McLaughlin, M.R. Mumpower, G. Savard, R. Surman, A. Aprahamian, F. Buchinger, M.T. Burkey, D.A. Gorelov, T.Y. Hirsh, J.W. Klimes, G.E. Morgan, A. Nystrom, and K.S. Sharma, *Phys. Rev. Lett.* **120**, 262702 (2018).
- [10] K. Siegl, K. Kolos, N. D. Scielzo, A. Aprahamian, G. Savard, M. T. Burkey, M. P. Carpenter, P. Chowdhury, J. A. Clark, P. Copp, G. J. Lane, C. J. Lister, S. T. Marley, E. A. McCutchan, A. J. Mitchell, J. Rohrer, M. L. Smith, and S. Zhu, *Phys. Rev. C* **98**, 054307 (2018).
- [11] D. J. Hartley, F. G. Kondev, G. Savard, J. A. Clark, A. D. Ayangeakaa, S. Bottoni, M. P. Carpenter, P. Copp, K. Hicks, C. R. Hoffman, R. V. F. Janssens, T. Lauritsen, R. Orford, J. Sethi, and S. Zhu, *Phys. Rev. C* **101**, 044301 (2020).
- [12] G. Savard, M. Carpenter, and J. Song, DOE proposal (2019).
- [13] H. Iwase, K. Nitta, and T. Nakamura, *J. Nucl. Sci. Technol.* **39**, 1142 (2002).
- [14] J. Reijonen, K.-N. Leung, R. B. Firestone, J. A. English, D. L. Perry, A. Smith, F. Gicquel, M. Sun, H. Koivunoro, T.-P. Lou, B. Bandong, G. Garabedian, Zs. Revay, L. Szentmiklosi, and G. Molnar, *Nucl. Instrum. Methods Phys. Res. A* **522**, 598 (2004).
- [15] A. Burlon, A. J. Kreiner, A. A. Valda, D. M. Minsky, H. R. Somacal, M. E. Debray, and P. Stolia, *Nucl. Instrum. Methods Phys. Res. B* **229**, 144 (2005).
- [16] H. Tran, A. Marchix, A. Letourneau, N. Chauvin, A. Menelle, F. Ott, and J. Schwindling, *J. Phys.: Conf. Ser.* **1021**, 012008 (2018).
- [17] H. Liskien and A. Paulsen, *At. Data Nucl. Data Tables* **15**, 57 (1975).
- [18] K. Shibata, O. Iwamoto, T. Nakagawa, N. Iwamoto, A. Ichihara, S. Kunieda, S. Chiba, J. Katakura, and N. Otuka, *J. Korean Phys. Soc.* **59**, 1046 (2011).
- [19] D. Brown *et al.*, *Nucl. Data Sheets* **148**, 1 (2018).
- [20] E. Crouch, *At. Data Nucl. Data Tables* **19**, 417 (1977).
- [21] Brookhaven National Laboratory National Nuclear Data Center, www.nndc.bnl.gov (2008).
- [22] Idaho National Laboratory Catalog, gamma.inl.gov.
- [23] D. Radford, *Nucl. Instrum. Methods Phys. Res. A* **361**, 297 (1995).
- [24] J. Hubbell and S. Seltzer, X-ray mass attenuation coefficients, <http://physics.nist.gov/PhysRefData/XrayMassCoef/cover.html> (1995).
- [25] A. Santamirina *et al.*, *JEFF Report 22* (2009).
- [26] B. B. Back and A. H. Wuosmaa, *Nucl. Phys. News* **23**, 21 (2013).